Plant Physiology and Biochemistry 139 (2019) 66–81

Contents lists available at ScienceDirect

Plant Physiology and Biochemistry

journal homepage: www.elsevier.com/locate/plaphy

Research article

miRNAs associated with auxin signaling, stress response, and cellular activities mediate adventitious root formation in apple rootstocks

Ke Li, Zhen Liu, Libo Xing, Yanhong Wei, Jiangping Mao, Yuan Meng, Lu Bao, Mingyu Han, Caiping Zhao**, Dong Zhang*

Department of Horticulture College, Northwest Agriculture & Forestry University, Yangling, 712100, China

ARTICLE INFO

Keywords:
Malus domestica
Adventitious root
Rootstock
Hormone
Transcriptome
Degradome sequencing
miRNA

ABSTRACT

Adventitious root (AR) formation is essential for the vegetative propagation of apple rootstocks. miRNAs play a significant role in regulating AR development, however, large-scale transcriptomic data on miRNA mediated AR formation in apple rootstocks is lacking. Therefore, in order to identify the molecular mechanisms underlying AR formation in 'M9-T337' apple rootstocks, transcriptomic changes occurring during key time points of AR formation (0, 3, and 16 days) were analyzed using high-throughput sequencing with a focus on miRNAs. A total of 84 known miRNAs and 56 novel miRNAs have differentially expressed were identified. Additionally, a total of 88 target genes of known miRNAs and 76 target genes of novel miRNAs were identified by degradome sequencing. The expression levels of the miRNAs and target genes were quantified by RT-qPCR. Results indicate that miRNAs and their target genes are associated with auxin signal-related (miR160 and miR390), stress response-related (miR398, miR395 and miR408), cell fate transformation-, proliferation- and enlargement-related (miR171, miR156, miR166, miR319 and miR396). These all involve pathways that participate in AR formation in 'M9-T337' apple rootstock. In addition, hormones (AUX, CTK, GA3, BR, JA, and ABA) are also involved in regulating AR formation. The candidate genes belonging to pathways associated with AR formation exhibited significantly higher expression levels, providing evidence that they may be involved in the regulation of AR development. The collective results of the present study indicate that the developmental process associated with AR formation in apple rootstock is extremely complex. The known and novel miRNAs and target genes that were identified by high-throughput and degradome sequencing, respectively, provide a framework for the future analysis of miRNAs associated with AR development in apple rootstocks, and provide new information that can be used to better understand AR development in woody plants.

1. Introduction

Apple (*Malus x domestica Borkh.*) is a widely consumed fruit crop worldwide, and China is the leading apple-producing country. There has been a major breakthrough in the development of dwarf and compact planting techniques for the modern apple industry in recent decades. The 'M9-T337'dwarfing apple rootstock is widely used and confers early fruiting and high yields. In order to maintain the genetic uniformity of rootstocks, the vegetative propagated method of mound layering and cutting propagation are widely used and the ability of AR formation plays a key role in that process. Breeding of dwarf rootstocks appropriate for the needs of the apple industry in China, however, has been a bottleneck. Therefore, the study of the molecular mechanisms of AR formation has both important theoretical and practical value for apple rootstock breeding and improvement.

AR formation is a complex process that emerges from stems, leaves or hypocotyls, being strategic for clonal propagation, and ARs may develop spontaneously, upon environmental stress or hormonal treatment; auxins strongly influence AR (Da Costa et al., 2018). A synthetic form of auxin, NAA and 2, 4-D also are widely used to induce AR formation in cuttings plants (Da Costa et al., 2018). In addition, stress signals are also important factors in AR formation. For example, a series of stress signal induced by injury results in the accumulation of endogenous auxin, triggering a series of cell cycle reactions (Zhou et al.,

* Corresponding author.
** Corresponding author.
E-mail addresses: keli505@163.com (K. Li), zlhieun@nwafu.edu.cn (Z. Liu), libo_xing@nwafu.edu.cn (L. Xing), 1551882256@qq.com (Y. Wei), mjp588@nwafu.edu.cn (J. Mao), myhh0430@nwafu.edu.cn (Y. Meng), baolu@nwsuaf.edu.cn (L. Bao), hanmy@nwsuaf.edu.cn (M. Han), zhcc@nwsuaf.edu.cn (C. Zhao), afant@nwsuaf.edu.cn (D. Zhang).

https://doi.org/10.1016/j.plaphy.2019.03.006
Received 5 September 2018; Received in revised form 27 January 2019; Accepted 5 March 2019
Available online 08 March 2019

2018). However, the mechanism of AR formation is unclear, and still need further study.

MiRNAs play an important role in regulating plant development (Yan et al., 2018). Individual miRNAs, however, cannot regulate root development but rather must be associated with their target genes. For example, miR160 functions as a key controller of root cap cell formation, and also targets *ARF17* to regulate AR initiation (Gutierrez et al., 2009). miR390, TAS3-derived trans-acting short-interfering RNAs (tasiRNAs), and *ARFs* form an auxin-responsive regulatory network that controls lateral root initiation and growth (Marin et al., 2010). In addition, the interaction of miR393 with *TIR1* (transport inhibitor response protein 1) modulates auxin sensitivity and affects primary root growth and lateral root emergence (Chen et al., 2011). Recently, a novel regulatory pathway involving bidirectional cell signaling mediated by miR165/miR166 and the transcription factors *SHR* (SHORT ROOT)/SCR (SCARECROW) has been identified as determining root cell fate (Carlsbecker et al., 2010). Elevated levels of miR156 promote adventitious root formation in maize, tomato, and tobacco (Feng et al., 2016). Overall, development of the root is clearly a dynamic process that requires the integration of plant hormones, transcriptional regulators, and small RNAs to produce the correct developmental outcome (Meng et al., 2010). While the mentioned studies reveal the initial mechanism of AR initiation by some specific miRNAs, studies on the genome-wide identification of miRNAs regulating AR development in apple rootstocks is still lacking.

The main objective of the current study was to provide a framework of miRNAs associated with AR development in apple rootstocks at a whole genome level. High-throughput sequencing and a degradome library were used to identify miRNAs and their targets genes, respectively, which were associated with AR formation in 'M9-T337' apple rootstocks. Hormone levels were also monitored. The combined analyses were used to provide the first global monitoring of changes occurring in the expression levels of miRNAs during AR formation in 'M9-T337' apple rootstocks. These findings contribute to the basic understanding of the molecular events underlying AR formation in apple rootstocks and provide direction for future research on AR formation in woody species.

2. Material and methods

2.1. Plant material

Micro-propagated 'M9-T337' apple rootstock plantlets were grown in tissue culture at the Northwest Agriculture and Forestry University, Yangling, China. The tissue culture cuttings were maintained under a 16 h light at 25 ± 1 °C, followed by 8 h dark at 15 ± 1 °C. Stems of the microcuttings were treated with indole-3-butyric acid (IBA), which is widely used to promote adventitious rooting. The rooting medium was composed of 1/2 MS, 1 mg.L-1 IBA, 20 g.L-1 sugar and 8 g.L-1 agar, pH 5.8. The medium without IBA was used to grow non-IBA treated, control plants. A total of 540 uniform cuttings were selected and sampled at the three time points: 0 days (S0), 3 days (S1), and 16 days (S2); representing the 0 day, 3 days, and 16 days after the transfer of the cuttings to the medium, respectively. A part of the group samples with IBA-treated were used for RNA-seq; the latter group samples without IBA-treated serving as controls. Three biological replicates were used in the analysis and a total of 180 uniform cuttings were sampled at each time point. Samples consisted of a basal portion of the stems (approximately 0.5 cm) containing the AR zone. The collected samples were immediately immersed in liquid nitrogen and stored at −80 °C until used for further processing.

2.2. Determination of hormone levels

Indole-3-acetic acid (IAA), zeatin riboside (ZR), Gibberellic acid 3 (GA3), Brassinolide (BR), Jasmonic acid (JA), and Abscisic acid (ABA) contents between stem cuttings harvested from IBA-treatment and control. Approximately 0.6 g fresh weight of stems collected during the AR formation and levels were determined using an indirect ELISA technique which was conducted at the Center of Plant Growth Regulator, China Agricultural University as described by Zuo et al., (2018). Detailed descriptions of the extraction and quantification methods are provided in our previous research (Fan et al., 2016). Three biological replicates were used for each hormone analysis (200 mg per replicate).

2.3. RNA library construction and high-throughput sequencing

RNA library construction followed the methods described in Xing et al. (2014). Total RNA was extracted at the three key time points of AR formation (0, 3, and 16 days). RNA extracts were obtained from three biological replicates (60 cuttings per replicate, totaling 180 cuttings) at each of the time points using the RNeasy Plant Mini Kit (Qiagen, Hilden, Germany). The RNA from each of the pooled extracts was used for small RNA library construction. The small RNAs with adapters were transcribed into cDNA using Super-Script II Reverse Transcriptase (Invitrogen, Shanghai, China). Lastly, the cDNA products were amplified by PCR and the purified PCR products were then sequenced by the Biomarker Biotechnology Corporation (Beijing, China) using an Illumina Genome Analyzer HiSeq2500. Total RNA from each of the pooled samples at the three time points was also used for degradome library construction and sequencing.

2.4. Profiling and differential expression analysis of known and novel mirRNAs

The criteria for the sequence quality control was based on the studies of Xing et al. (2014) and included: 1) The removal of low-quality reads (base mass below 30 in more than 20% of the sequences); 2) removal of reads containing unknown bases (N) greater than or equal to 10% of the sequence; 3) removal of the 3 'end connector and barcode sequence; and, 4) removal of sequences shorter than 18 nt or longer than 30 nt. Sequence alignment and subsequent analysis were performed using the *Malus x domestica* Whole Genome v1.0p Assembly (ftp://ftp.ncbi.nlm.nih.gov/genomes/all/GCF_000148765.1_MalDomGD1.0/GCF_000148765.1_MalDomGD1.0_genomic.fna.gz) as a reference genome. miRDeep2 (Friedlander et al., 2012) software was used to compare unannotated reads with the reference genome to obtain position information within the reference genome, in order to map the unannotated reads.

DESeq (http://precedings.nature.com/documents/4282/version/2) was used to differentially expressed miRNAs. The criteria for defining differential expression of miRNAs were $|\log2\ (FC)| \geq 1$ (Fold Change, FC) and FDR ≤ 0.01 (False Discovery Rate, FDR). Fold Change (FC) represents the ratio of the expression between two samples (groups). In addition, the accepted Benjamini-Hochberg correction method was used to correct the p value (p-value) of the original hypothesis test, and the false discovery rate (FDR) was used as the key index for initially identifying differentially expressed miRNAs.

2.5. Prediction, identification, and annotation of targets of miRNA

TargetFinder (http://carringtonlab.org/resources/targetfinder) software was used to predict the potential targets of both the known and novel miRNAs by matching the miRNA sequences to the apple genome (*Malus x domestica* Borkh.). In addition, Some targets of known and novel miRNAs were identified by degradome sequencing, which the degraded fragments were matched to the apple genome (*Malus x domestica* Borkh) after the removal of ncRNAs and polyN fragments in order to reduce interference (Xing et al., 2014). Shear site detection was performed using Cleaveland software (Addoquaye et al., 2009). Set condition P-value < 0.05. Sequence alignment of target genes with NR,

Swiss-Prot, GO, KEGG, COG databases using BLAST software, obtain annotation information for the target genes.

2.6. RT-qPCR analysis of the expression levels of putative miRNA and target genes

The expression patterns of candidate DEGs, including auxin-, stress response-, and cell fate-, and AR formation-related genes, were validated by RT-qPCR. The sequences of the designed primer pairs were selected based on apple data (*Malus* × *domestica*) that were published in GenBank using Primer 6.0 software. RT-qPCR was conducted as described in previous research (Xing et al., 2014). An apple *ACTIN* gene was used for normalization. Each of the analyzed samples consisted of three biological and technical replicates. The $2^{-\Delta\Delta}$Ct method was used to calculate the relative expression of the analyzed genes (Livak and Schmittgen, 2001). The sequences of the utilized the gene-specific primers are listed in Table S1.

2.7. Statistical analysis

Differences among means were evaluated with the Statistical Program for Social Science 19 (SPSS19, Chicago, IL, USA) using a two-tailed *t*-test at the 5% level. Statistical processing of plant phenotype data, hormone content, and RT-qPCR data was performed in Microsoft Excel (2010). Diagrams were generated in Microsoft Excel (2010) and OriginPro 7.5 (OriginLab Software, Inc.).

3. Results

3.1. IBA-induced changes in morphology and hormone levels during AR formation

The outline of ARs could be observed at the stem base during the elongation phase when the callus tissue expanded into a spheroid shape. Callus formation was observed at S1 (Fig. 1A). Indole-3-acetic acid (IAA) and zeatin riboside (ZR), an endogenous auxin and cytokinin, respectively, were the most abundant hormones measured. IAA and ZR levels were relatively higher at S1 and S2 than at S0 (Fig. 1B). GA content was highest at S1, while no significant difference between S0 and S2 (Fig. 1B). ABA, a stress-response hormone, increased significantly from S0 to S1 but no difference was observed between S1 and S2 (Fig. 1B). BR content significantly increased from S0 to S2, but JA content significantly decreased over the same period of time (Fig. 1B). The ratio of IAA/ZR at S2, however, was significantly lower than at S0 (Fig. 1C). The ratio of IAA to ABA exhibited a similar to the trend observed in the IAA/ZR ratio, while the ABA/GA ratio steadily during the entire AR formation sampling period (Fig. 1C). The different levels of hormones and changes in the ratios reflect their various functions during specific phases of AR development.

3.2. Construction and sequencing of the small RNA libraries

A total of 446,150,025 raw reads were obtained via high-throughput sequencing. The average numbers of raw reads at each time points were 53,703,123 at S0, 48,113,652 at S1, and 46,899,901 at S2 (Table S2). After removal of low quality reads, a total of 289,363,684 (64.86%) clean reads were selected from nine libraries (Table S2). A degradome library derived from mixed total RNA from the three key time points (S0, S1 and S2) was constructed and a total of 13,439,101 raw tags were generated, resulting in 13,410,565 (99.79%) clean tags and 4,783,127(35.59%) unique tags (Table S3). The clean reads were categorized into rRNA, scRNA, snRNA, snoRNA, tRNA, Repbase, mapped reads and unmapped reads. Detailed information on the libraries is presented in Table S4.

3.3. Identification of known miRNAs and their expression patterns

A total of 190 known miRNAs belonging to 39 miRNA families were identified (Fig. S1). The mature sequences of the identified known miRNAs are listed in the database. The number of known miRNAs in different families varied significantly, from 1 (mdm-miR1511, 391, 535, 7125, 827 and 858) to 31 (mdm-miR156) (Fig. S1).

The expression levels of known miRNAs in the nine libraries were determined by the number of their read counts. The miRNAs were classed into one of six categories based on their reads counts (Fig. S2). Moderate expression (100–999 reads) contained the largest number of miRNAs at S0 but the low expression (10–99 reads) category was the largest at S1 and S2 (Fig. S2). After normalization, the identified known miRNAs were hierarchical clustered based on the TPM values to display their expression abundance (Fig. 2A). Some miRNAs had very high expression levels, with more than 10,000 read counts, including mdm-miR398b/c, miR408s and miR319a/b, (Fig. S2 and Fig. 2A), while others had very low expression levels, with less than 10 reads, including, miR398a, miR319c, miR7125; as well as some of the mdm-miR156, miR399, and miR171 family members (Fig. S2 and Fig. 2A).

3.4. The identification of known miRNAs that are differentially expressed during AR formation

A total of 84 known miRNAs, were identified. Among these miRNAs, 74 were down-regulated (including mdm-miR398a, miR156aa, and miR160a etc); and 10 miRNAs were up-regulated (including mdm-miR390a, miR396a, and miR3627a-c etc) (Figs. 2B and 3). The values of $\log_2$FC of the known miRNAs were in the range of −5.36 to 4.00, with miR390 exhibiting the largest increase; while miR398a exhibited the smallest decrease (Fig. 3).

The Venn diagram illustrates the number of known miRNAs showed that a total of 65 miRNAs were differentially expressed in the initiation phase (S0 vs S1), 11 in the elongation phase (S1 vs S2), and 69 over the whole time course of AR formation (S0 vs S2) (Fig. S3A). More specifically 12, miRNAs were only up-regulated, 66 miRNAs were only down-regulated, and 9 miRNAs were both up- and down-regulated over the course of AR formation (Fig. S3B).

3.5. Identification of putative novel miRNAs, that were differentially expressed during AR formation

The novel miRNAs had relatively lower levels of expression. The largest percentage of novel miRNAs fell into the very low category (1–9 reads) and the percentages varied from 35.08% to 40.74% in the different libraries. This was followed by those that fell into the low category (10–99 reads) and the percentages in each library varied from 23.52% to 35.49%. There were few novel miRNAs (< 4.123%) that exhibited more than 1000 reads (Fig. S4).

The Venn diagram illustrates that 56 novel miRNAs were differentially (Fig. S5). Among all of the novel miRNAs, 28 miRNAs were only differentially expressed in S0 vs S1, and 4 within S1 vs S2. In addition, 25 miRNAs were only down-regulated, and 31 miRNAs were only up-regulated. None of the novel miRNAs exhibited both up- and down-regulated over the course of AR formation (Fig. S5B). The relative expression level of each novel miRNA is indicated by the blue-white-red gradient colors. The hierarchical clustering of the 56 novel miRNAs showed three major clusters (Fig. 4).

3.6. Degradome sequencing identification of target genes of the known and novel miRNAs

The results of targets of known and novel miRNAs analyzed by degradome sequencing were showed in Tables 1 and 2. After merging the miRNAs with their corresponding mature sequence, a total of 91 miRNAs with 144 target genes and 203 cleavage sites were found in the

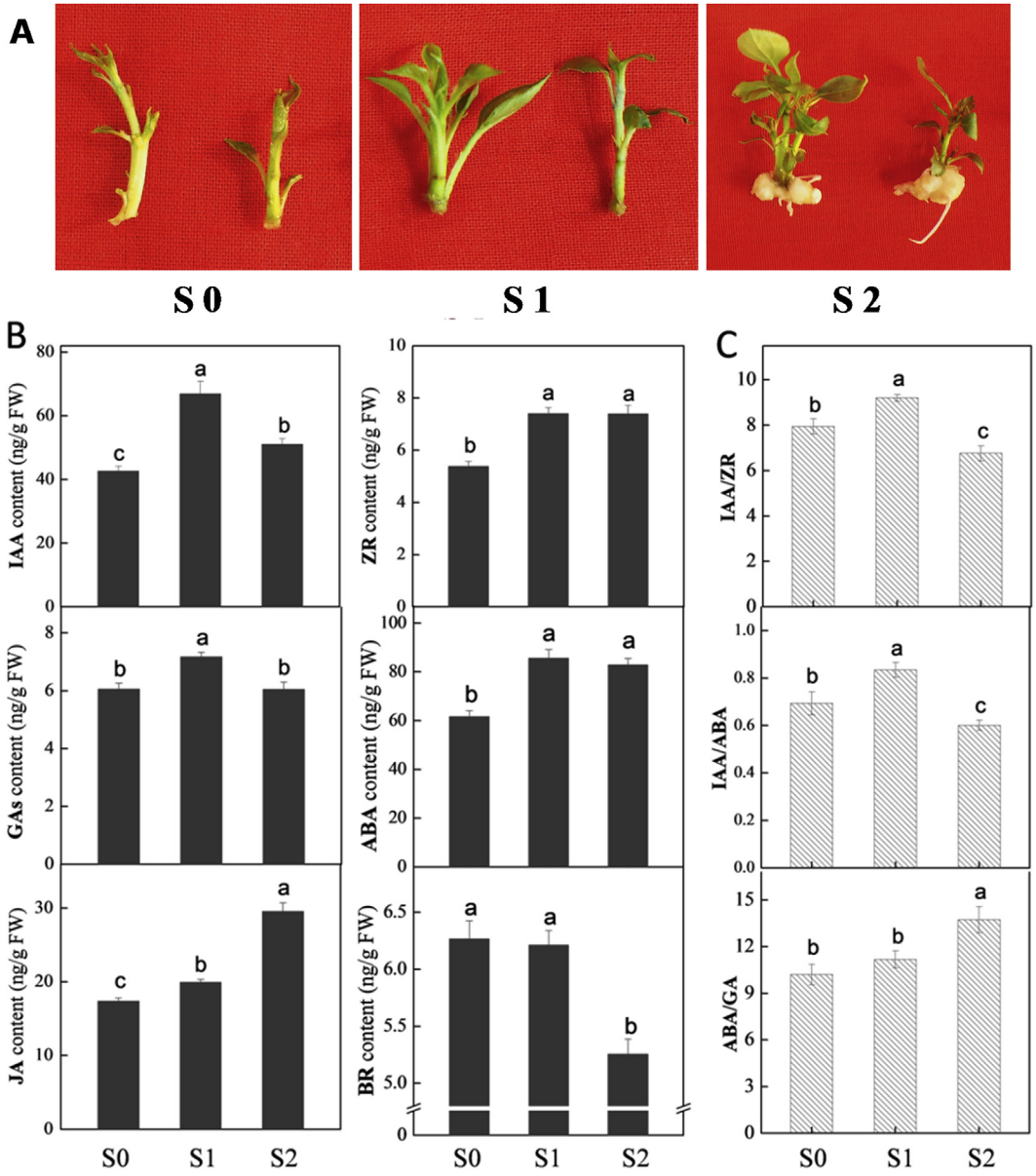

Fig. 1. Time course and the hormone contents in the AR formation of 'M9-T337' apple root stocks. (A) Time course of AR formation: S0 indicates the initial placing of the apple cuttings into rooting medium (0 day after transplantation); S2 indicates that the callus tissue shows up at the base of the cuttings (about 9 days after transplantation); S3 indicates that the AR stretches out (about 16 days after transplantation). (B) IAA: Indole-3-acetic acid; ZR: zeatin riboside; GA: gibberellin; ABA: abscisic acid; JA: jasmonic acid; BR: brassinolide. (C) Ratios of hormone contents: IAA/ZR, IAA/ABA and ABA/GA. Bars show SD with three biological replicates. Values represent means ± SE (n = 3). The statistical analysis was performed by Duncan's multiple range test at level $p \leq 0.05$.

degradome library (P-value < 0.05), and examples of the specific cleavage sites in the genes could be observed (Fig. S6). Most of the targets in the GO annotation were placed in the binding category of molecular function and the cellular category of biological process. A total of 82 known miRNA members belonging to 20 miRNA families (including miR156, 160, 166, 171 and 396) and 88 targets were identified (Table 1). The majority of the known miRNAs identified in the current study could potentially regulate multiple target genes. For example, mdm-miR156 regulates *SPL6, SPL13B,* and *ACOS5*, mdm-miR319 regulates *TCP2* and *TCP4*, and mdm-miR396 regulates *GRF1*, *GRF2,* and *GRF5*. Mdm-miR160 regulates *ARF16* and *ARF17* (Table 1), and the cleavage site information for miR160 with its targets is presented in Fig. S7.

A total of 56 novel miRNAs and 76 targets were identified. After filtering out the miRNAs that fell into the no expression (0 read) category and the very low (1–9 reads) category (Fig. S4), and then the novel miRNAs with higher category were analyzed in Table 2. The targets of the novel miRNAs included genes (encoding regulatory proteins) and transcription factors (TFs), such as *TCPs* and the cytochrome P450 superfamily (Table 2). The targets of novel miRNAs have multiple functional typles. Some of the targets were associated with phytohormone pathways, such as *BSK2* (target of chr1_1772328) in BR signaling, *IAA9* (target of chr5_2661918) in auxin signaling (Table 2). There were also some targets of that respond to stress signals, including *CYP94B3* (chr3_2294129) in wounding signals, and *DREB2C* (chr1_1772328) in drought stress, etc (Table 2).

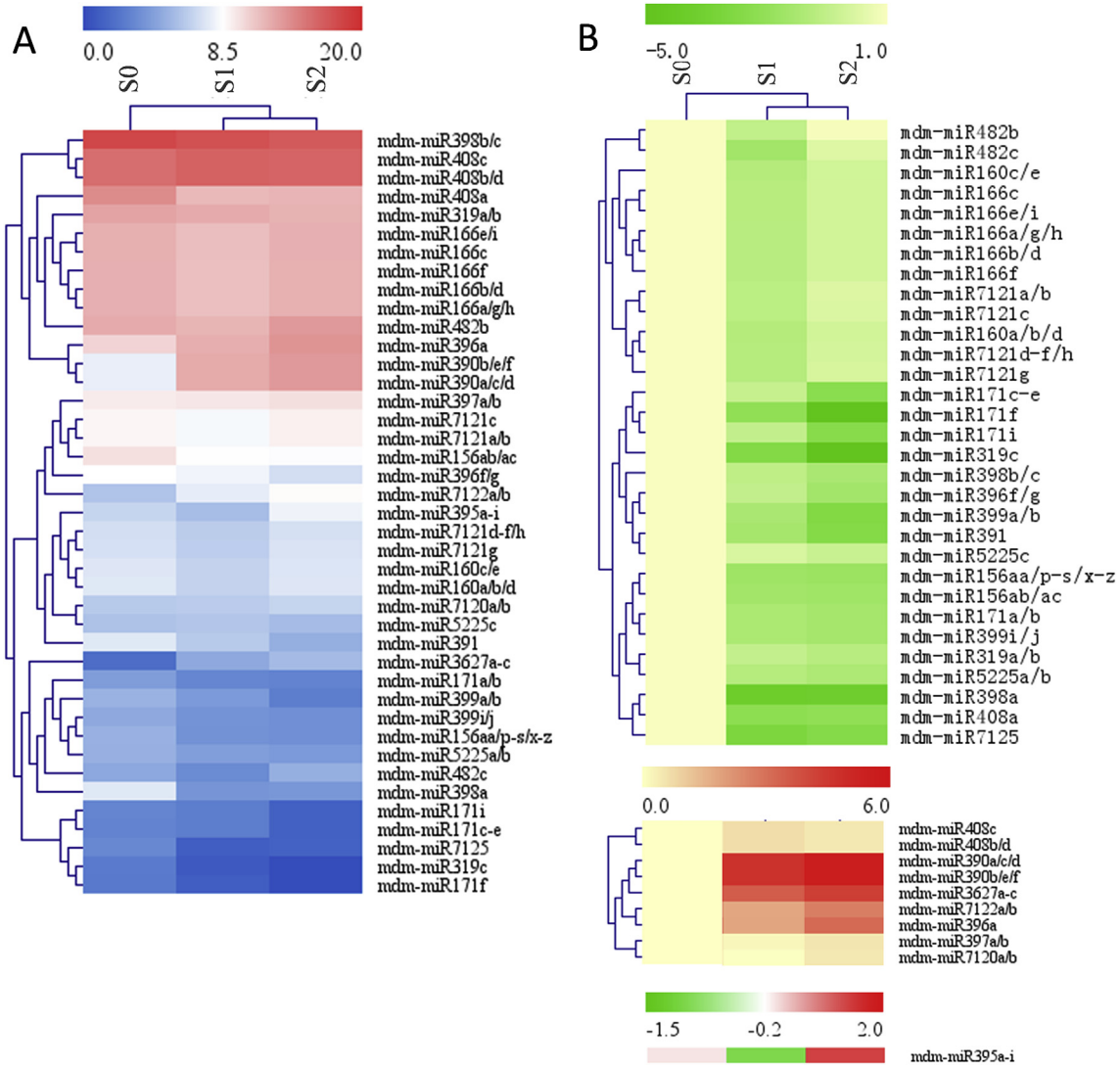

Fig. 2. Hierarchical clustering of differently expressed known miRNAs in AR formation process. (A) Heat map diagram of $\log_2$ (TPM + 1) values for known miRNAs. The distance metric of hierarchical clustering was Euclidean Distance. (B) Heat map diagram of down-regulated, up-regulated and both up-and down-regulated miRNAs in differentially expressed miRNAs library. Make the TPM value of S0 was parameter. The distance metric of hierarchical clustering was Pearson Correlation.

3.7. RT-qPCR analysis of differentially expressed miRNAs and targets during AR formation that are associated with auxin signaling

The expression levels of miRNAs (miR160 and miR390) and their targets, which were associated with auxin signaling, were examined by RT-qPCR (Fig. 5). The targets of miR160 and miR390 are AUXIN RESPONSE FACTORS (*ARF*s). The expression level of miR160a exhibits a significant decrease from S0 to S1, followed by an increase from S1 to S2. In contrast, the target gene, *ARF16*, displays its highest expression level at S1 (Fig. 5A). MiR390a increased by 8-folds from S0 to S2. However, the target gene of miR390a, *ARF3*, exhibited its lowest expression level at S2 (Fig. 5B). The expression patterns of miRNAs (miR160a, miR390a) and targets (*ARF16, ARF3*) are quite opposite. Results from the RT-qPCR analysis indicated that the expression patterns of miR160 and miR390 were largely consistent with the data obtained from RNA-seq data (Fig. 5). This collective evidence further suggests that the miRNAs and their targets that are associated with auxin signaling may play a role in regulating AR formation in 'M9-T337' apple rootstocks.

3.8. RT-qPCR analysis of differentially expressed miRNAs and their targets during AR formation that are associated with stress response and signal transduction

The expression level during AR formation of four miRNAs and their target genes, which are associated with stress response and signal transduction, were examined by RT-qPCR (Fig. 6). The expression profiles of miR398a, miR398b and miR408a exhibited a down-regulation pattern from S0 to S2 (Fig. 6B–D). However, the expression level of miR395a increased from S0 to S2 (Fig. 6A). The target gene of miR395a, *APS1*, reached its maximum at S1 (Fig. 6A). The target gene of miR398a and miR398b (*CSD2*, *PYL4* and *SP1L*) gradually increased in expression from S0 to S2 (Fig. 6B C). The expression level of miR408a decreased by approximately 80% from S0 to S1, and stayed relatively low level at S2. *DegP9* and *ARPN,* the target genes of miR408a, however, exhibited variable expression patterns during AR formation (Fig. 6D). Although the expression levels of miRNAs at several data points varied between RNA-seq and qRT-PCR, the differential expression trends detected by the two approaches were largely consistent (Fig. 6).

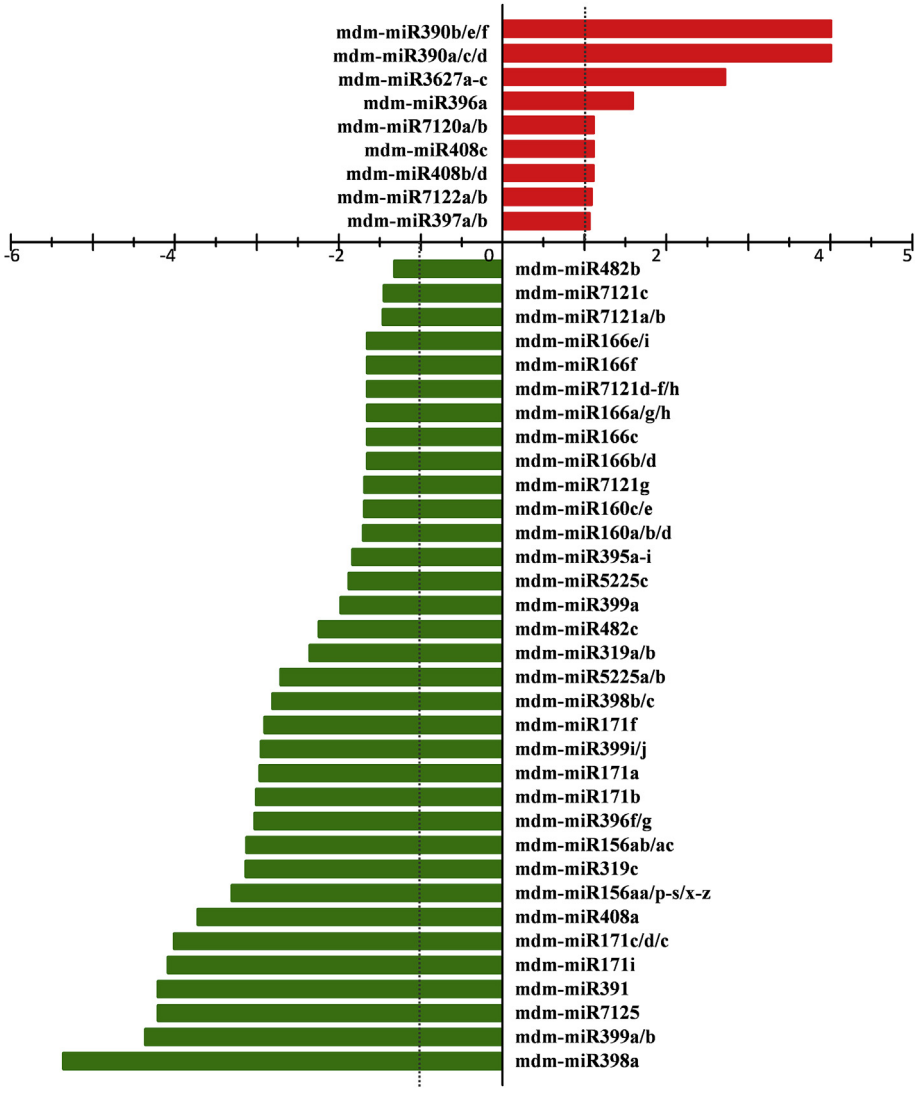

Fig. 3. Fold-Change of differently expressed known miRNAs. The red bars refer to $\log_2$FC of up-regulated miRNAs, and green ones to the down-regulated miRNAs. Vertical dotted lines refer to the screening criteria: |log2(FC)| = 1. (For interpretation of the references to color in this figure legend, the reader is referred to the Web version of this article.)

3.9. RT-qPCR analysis of differentially expressed miRNAs and their targets during AR formation that are associated with cell fate transformation, proliferation, and enlargement

The expression levels of miRNAs and target genes that associated with cell fate transformation, proliferation and enlargement were examined by qRT-PCR. RT-qPCR analysis indicated that the expression of miR171a and miR319a exhibited its lowest expression level at S1, while its target genes (*HAM3, TCP2 and TCP4*) exhibited its highest expression level at S1 (Fig. 7A D). The expression level of mdm-miR156ab was down-regulated from S0 to S2, while the target genes (*SPL6 and SPL13B*) exhibited an opposite trend to mdm-miR156ab in expression (Fig. 7B). The expression level of miR166a significantly decreased from S0 to S2, while the target gene, *PHB* and *REV*, reached its maximum at S1 (Fig. 7C). The expression profiles of miR396a and miR396f were different from each other. MiR396a was up-regulated from S0 to S1 and decreased from S1 to S2. However, the relative expression level of miR396f was significantly down-regulated from S0 to S2 (Fig. 7E). Their target gene, *GRF1,* significantly increased from S0 to S1 but did not exhibit any significant difference in expression between S0 and S2 (Fig. 7E). In general, the RT-qPCR results were largely consistent with the data obtained from miRNAs sequencing TPM (Fig. 7).

3.10. RT-qPCR analysis of differentially expressed genes associated with pathways related to AR formation

The expression profiles of several genes that are specifically associated with AR formation were analyzed by RT-qPCR. The selected genes could be classified as auxin-related, cytokinin-related, cell cycle-related, root development-related, etc (Fig. 8). Among all of the selected genes, *IAA3* exhibited its highest expression level at S1. the expression profiles of *PIN1*, *PLT* and *RR12* showed significantly decreased from S0 to S1 and no significant difference between S1 and S2 (Fig. 8A). The expression level of *IPT1-2, CYCD1;1 and CYCP4;1* exhibited its lowest expression level at S1 and no significant difference between S0 and S2 (Fig. 8). *ACO1* and *JAZ12* are stress-signal response genes and their expression levels were significantly up-regulated (from S0 to S2) (Fig. 8A). The expression level of *WOX5, LRP1,* and *SCR1* were up-regulated during AR formation (Fig. 8B). The expression profile of *RHS19,* however, was opposite to *SCR1* (Fig. 8B).

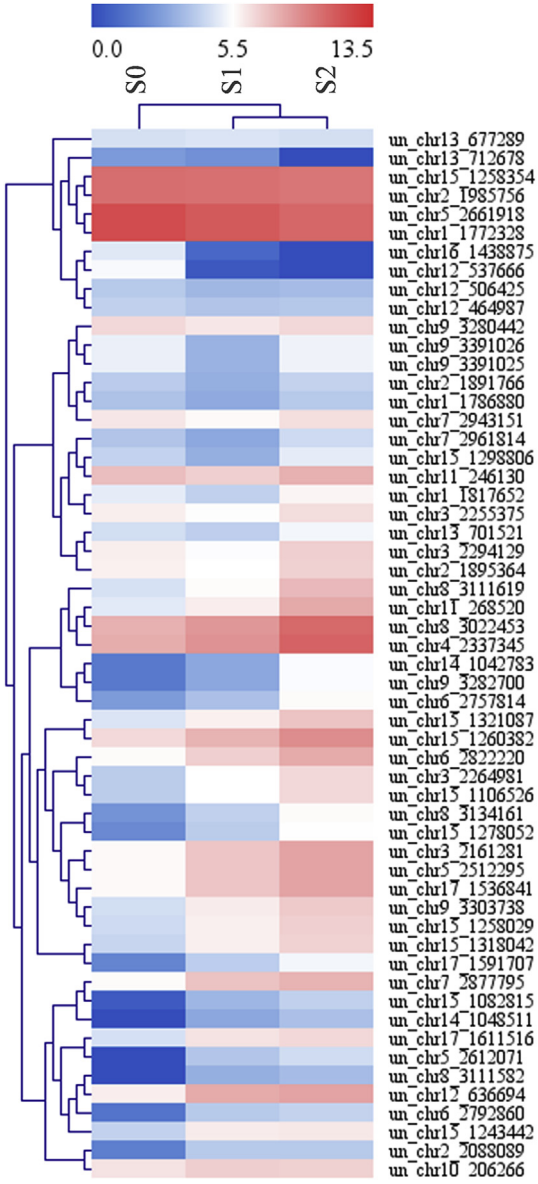

Fig. 4. Hierarchical clustering of differently expressed novel miRNAs in AR formation process. Heat map diagram of $\log_2$ (TPM + 1) values for differently expressed novel miRNAs. The distance metric of hierarchical clustering was Pearson Correlation.

4. Discussion

4.1. Hormone levels

Hormones play a crucial role in plant development and the interaction networks determines the capacity, position, and efficiency of AR formation (Negishi et al., 2014). The accumulation of auxin in the stem above the point of cutting is absolutely required for AR induction, but inhibits AR elongation (Sukumar et al., 2013) (Fig. 1B). The expression profiles of auxin-associated genes are approximately in accordance with the accumulation of auxin during the AR induction phase. These factors may be the reason why species with difficult to rooting are treated with exogenous auxin during the induction phase of AR formation in production.

In contrast to auxin, cytokinins (CTK) play a suppressive role during AR induction phase but promote cell division and differentiation during the extension phase of AR formation (Dello Ioio et al., 2012). A critical factor regulating AR development is the ratio of auxin to cytokinin. The cuttings used in this study did not have any primary roots (organs that favor an accumulation of CTK) which promoted a higher IAA/CTK ratio and thus also promoted the initiation and growth of AR (Rani and Taketa, 2005). The interaction and balance between auxin and cytokinin mediates AR formation. In the current study, the levels of JA, GA, ABA and BR also have changed during AR formation in apple rootstock. Collectively, the data on hormone patterns indicate that AR development is a complex process affected by various types of hormonal regulation. However, the mechanisms underlying and associated with their interaction, remain to be further experimentally demonstrated.

4.2. MiRNAs and their targets that are associated with auxin signaling pathways are involved in regulating AR formation in apple rootstocks

Auxin-related miRNAs were identified in the present study, including miR160 and miR390. The target gene of miR160 is *ARF*, which regulates the expression of auxin-responsive genes by binding to auxin response elements (AuxREs) in the promoters. MiR160 inhibits callus initiation from pericycle-like cells, while *ARF10* promotes it (Liu et al., 2016). In addition, over-expression of miR160c resulted in a phenotype characterized by shorter and more gravitropic roots with an enlarged tumor-like apex (Wang et al., 2005). In the present study, the expression profiles of miR160a and *ARF16* are consistent with these previous reports. Therefore, the involvement of miR160/ARFs in auxin signal response is readily apparent and may play a critical role in AR formation, although this will need to be confirmed by further studies.

MiR390 was also identified from the DEG library. In Arabidopsis, it has been reported that miR390 was specifically expressed at the sites of lateral root initiation where it triggers the biogenesis of tasiRNAs, followed by *ARF*-regulated lateral root growth (Marin et al., 2010). RT-qPCR results revealed that miR390a may be a positive regulator of AR development, but that *ARF3* had dual target genes (Fig. 5B). The results also indicated that miR390 has regulatory capacity over *ARFs*, but may act indirectly in that it is capable of cleaving the non-coding TAS3 precursor RNA to produce tasiRNAs, which can then cleave the transcripts of *ARF2*, *ARF3,* and *ARF4*. This may be the reason of miR390-ARF cleavage sites could not be detected in the degradome library. In addition, *ARF* genes also display overlapping expression domains, interact genetically and constitute a complex regulatory network, including feedback regulation (Gutierrez et al., 2009). In the current study, miR160 was confirmed to have a cleavage relationship with *ARF16* and *ARF17*, which might explain why miR390 and miR160 exhibited opposite expression patterns, even though they have similar targets (Fig. 5). Overall, the results indicate that miR160 and miR390 play a crucial role in AR formation and that the target genes of *ARFs* also act as key regulators of auxin signal transduction during AR formation in apple rootstocks. However, the mechanisms underlying and associated with their interaction remain to be further experimentally demonstrated.

4.3. MiRNAs and their targets that are associated with stress-response pathways are involved in regulating AR formation in apple rootstocks

Indeed, stress-response-related miRNAs were also identified in the present study, including miR398, miR395 and miR408.

Wounding is a primary stimulus for the induction of AR formation in the vegetative propagation of apple cuttings. The target gene of miR398 is *CSD2*, which belongs to subfamily of super oxide dismutase (SODs) (Fridovich, 1995). *CSD2* is also induced in response to wound response; and function to serve as the initial signal for AR formation (Steffens and Rasmussen, 2016). Therefore, we consider miR398a to be a rapid response miRNA in wounding-induced AR formation, which plays a primary role during the initial signal transmission.

In addition, miR395 targets *APS1* (ATP sulfurylase gene) which regulates sulfate accumulation and allocation in Arabidopsis (Liang et al., 2010). In Arabidopsis, sulfur nutrient availability has also been

Table 1
Detected targets of known miRNAs, some of their GO annotations and cleavage sites in 'M9-T337' apple rootstock AR formation.

known miRNAs	Targets					
	Gene ID	Description	GO annotation	GO ID	Alignment Range	Cleavage Site
156ab/ac/p-w	MDP0000119458, MDP0000193702	Squamosa promoter-binding protein-like (SBP domain) transcription factor family protein (AT1G69170.1, SPL6)	DNA binding	GO:0003677	1028–1048	1039
	MDP0000170630	Squamosa promoter-binding protein-like (SBP domain) transcription factor family protein (AT5G50670.1, SPL13B)	DNA binding	GO:0003677	770–790	781
	MDP0000249364	acyl-CoA synthetase 5 (AT1G62940.1, ACOS5)	4-coumarate-CoA ligase activity	GO:0016207	2714–2734	2725
159a/b	MDP0000147309	myb domain protein 65 (AT3G11440.1, MYB65)	chromatin binding	GO:0003682	954–973	964
160a-e	MDP0000131481	auxin response factor 16 (AT4G30080.1, ARF16)	response to hormone	GO:0009725	1506–1526	1517
	MDP0000221322	auxin response factor 16 (AT4G30080.1, ARF16)	auxin-activated signaling pathway	GO:0009734	1596–1616	1607
	MDP0000750392	auxin response factor 16 (AT4G30080.1, ARF16)	response to hormone	GO:0009725	1764–1784	1775
	MDP0000232116	auxin response factor 17 (AT1G77850.1, ARF17)	regulation of transcription, DNA-templated	GO:0006355	1302–1322	1313
	MDP0000256621	auxin response factor 17 (AT1G77850.1, ARF17)	response to hormone	GO:0009725	1611–1631	1622
	MDP0000273491	Co-chaperone GrpE family protein (AT1G36390.1)	chaperone binding	GO:0051087	300–320	311
162a/b	MDP0000187512	LETM1-like protein (AT3G11560.2)	Unknown	Unknown	1536–1556	1547
164b-f	MDP0000121265, MDP0000911724	NAC domain containing protein 100 (AT5G61430.1, ANAC100, ATNAC5, NAC100)	regulation of transcription, DNA-templated	GO:0006355	644–664	655
	MDP0000528658	NAC domain containing protein 1 (AT1G56010.2, anac021, ANAC022, NAC1)	regulation of transcription, DNA-templated	GO:0006355	527–547	538
166a-i	MDP0000050082, MDP0000943529	Homeobox-leucine zipper family protein/lipid-binding START domain-containing protein (AT2G34710.1, ATHB-14, ATHB14, PHB, PHB-1D)	sequence-specific DNA binding transcription factor activity	GO:0003700	587–607	598
	MDP0000126553	homeobox gene 8 (AT4G32880.1, ATHB-8, ATHB8, HB-8)	sequence-specific DNA binding transcription factor activity	GO:0003700	566–586	577
	MDP0000236500MDP0000242861 MDP0000426630	Homeobox-leucine zipper family protein/lipid-binding START domain-containing protein (AT5G60690.1, IFL, IFL1, REV)	sequence-specific DNA binding transcription factor activity	GO:0003700	560–580	571
	MDP0000251484	Homeobox-leucine zipper family protein/lipid-binding START domain-containing protein (AT1G52150.3, ATHB-15, ATHB15, CNA, ICU4)	sequence-specific DNA binding transcription factor activity	GO:0003700	605–625	616
	MDP0000313059	Homeobox-leucine zipper family protein/lipid-binding START domain-containing protein (AT1G52150.1, ATHB-15, ATHB15, CNA, ICU4)	sequence-specific DNA binding transcription factor activity	GO:0003700	551–571	562
	MDP0000336547	SGF29 tudor-like domain (AT3G27460.1)	Unknown	Unknown	311–332	322
	MDP0000005879	homeobox gene 8 (AT4G32880.1, ATHB-8, ATHB8, HB-8)	anatomical structure morphogenesis	GO:0009653	530–550	541
167b-j	MDP0000137461	auxin response factor 8 (AT5G37020.1, ARF8, ATARF8)	regulation of transcription, DNA-templated	GO:0006355	1182–1203	1193
	MDP0000232417	auxin response factor 8 (AT5G37020.1, ARF8, ATARF8)	response to hormone	GO:0009725	2418–2439	2429
	MDP0000153538	auxin response factor 6 (AT1G30330.1, ARF6)	response to hormone	GO:0009725	2388–2409	2399
	MDP0000319957	auxin response factor 6 (AT1G30330.2, ARF6)	response to hormone	GO:0009725	2682–2703	2693
	MDP0000550049	auxin response factor 6 (AT1G30330.2, ARF6)	response to hormone	GO:0009725	1917–1938	1928
169a-d	MDP0000195166	senescence associated gene 24 (AT1G66580.1, RPL10C, SAG24)	translation	GO:0006412	492–511	503
	MDP0000296077	nuclear factor Y, subunit A1 (ATHAP2A, EMB2220, HAP2A, NF-YA1, AT5G12840.1)	CCAAT-binding factor complex	GO:0016602	1631–1651	1642
171a/b/f/j-n	MDP0000151144	GRAS family transcription factor (AT4G00150.1, ATHAM3, HAM3)	regulation of transcription, DNA-templated	GO:0006355	1377–1397	1388
	MDP0000274120	GRAS family transcription factor (AT4G00150.1, ATHAM3, HAM3)	regulation of transcription, DNA-templated	GO:0006355	1905–1925	1916
	MDP0000275704	GRAS family transcription factor (AT4G00150.1, ATHAM3, HAM3)	regulation of transcription, DNA-templated	GO:0006355	1353–1373	1364
	MDP0000204187	XAP5 family protein (AT2G21150.1, XCT)	nucleus	GO:0005634	19–39	30

(*continued on next page*)

Table 1 (*continued*)

known miRNAs	Targets					
	Gene ID	Description	GO annotation	GO ID	Alignment Range	Cleavage Site
319a/b	MDP0000237553	TEOSINTE BRANCHED 1, cycloidea and PCF transcription factor 2 (AT4G18390.1, TCP2)	Unknown	Unknown	298–317	308
	MDP0000287069	TEOSINTE BRANCHED 1, cycloidea and PCF transcription factor 2 (AT4G18390.1, TCP2)	Unknown	Unknown	1180–1199	1190
	MDP0000763497, MDP0000920127, MDP0000927314	TEOSINTE BRANCHED 1, cycloidea and PCF transcription factor 2 (AT4G18390.1, TCP2)	Unknown	Unknown	1186–1205	1196
	MDP0000328318	TCP family transcription factor 4 (AT3G15030.1, MEE35, TCP4)	Unknown	Unknown	987–1007	998
	MDP0000442611	TCP family transcription factor 4 (AT3G15030.1, MEE35, TCP4)	Unknown	Unknown	840–860	851
393a-c	MDP0000125975	F-box/RNI-like superfamily protein (AT3G62980.1, TIR1)	cell cycle; auxin-activated signaling pathway; lateral root formation	GO:0007049; GO:0009734; GO:0010311	1505–1525	1516
	MDP0000203334	auxin signaling F-box 2 (AT3G26810.1, AFB2)	auxin-activated signaling pathway	GO:0009734	1858–1879	1870
	MDP0000469943	auxin signaling F-box 2 (AT3G26810.1, AFB2)	auxin-activated signaling pathway	GO:0009734	1120–1141	1132
	MDP0000498419	F-box/RNI-like superfamily protein (AT3G62980.1, TIR1)	cell cycle; auxin-activated signaling pathway; lateral root formation	GO:0007049; GO:0009734; GO:0010311	1523–1543	1534
395a-i	MDP0000121656	ATP sulfurylase 1 (AT3G22890.1 APS1)	Unknown	Unknown	334–354	345
	MDP0000263161	ATP sulfurylase 1 (AT3G22890.1 APS1)	Unknown	Unknown	1657–1677	1668
396a/b/f/g	MDP0000276970	growth-regulating factor 2 (AT4G37740.1, AtGRF2, GRF2)	regulation of transcription, DNA-templated	GO:0006355	372–393	383
	MDP0000125282	growth-regulating factor 1 (AT2G22840.1, AtGRF1, GRF1)	regulation of transcription, DNA-templated	GO:0006355	774–795	785
	MDP0000215583	growth-regulating factor 1 (AT2G22840.1, AtGRF1, GRF1)	regulation of transcription, DNA-templated	GO:0006355	753–774	764
	MDP0000274400	growth-regulating factor 5 (AT3G13960.1, AtGRF5, GRF5)	regulation of transcription, DNA-templated	GO:0006355	351–372	362
398a-c	MDP0000129223MDP0000193167	GroES-like zinc-binding dehydrogenase family protein (AT5G43940.1, ADH2, ATGSNOR1, GSNOR, HOT5, PAR2)	oxidation-reduction process	GO:0055114	35–55	46
	MDP0000156866	GroES-like zinc-binding dehydrogenase family protein (AT5G43940.2, ADH2, ATGSNOR1, GSNOR, HOT5, PAR2)	oxidation-reduction process	GO:0055114	75–95	86
	MDP0000250286	copper/zinc superoxide dismutase 2 (AT2G28190.1, CSD2, CZSOD2)	oxidation-reduction process	GO:0055114	429–450	440
	MDP0000258717	copper/zinc superoxide dismutase 2 (AT2G28190.1, CSD2, CZSOD2)	oxidation-reduction process	GO:0055114	441–462	452
	MDP0000290585	Integrase-type DNA-binding superfamily protein (AT2G40340.1, AtERF48, DREB2C)	sequence-specific DNA binding transcription factor activity	GO:0003700	592–612	603
	MDP0000387604	Unknown	Unknown	Unknown	141–161	152
	MDP0000530255	Ctr copper transporter family (AT2G26975.1)	copper ion transmembrane transporter activity	GO:0005375	33–54	44
	MDP0000683606	copper chaperone for SOD1 (AT1G12520.1, ATCCS, CCS)	oxidation-reduction process	GO:0055114	729–749	740
	MDP0000778113	Cupredoxin superfamily protein (AT1G71040.1, LPR2)	oxidation-reduction process	GO:0055114	823–843	834
	MDP0000228470	PYR1-like 4 (AT2G38310.1, PYL4, RCAR10)	response to biotic stimulus	GO:0009607	720–740	731
	MDP0000243217	SPIRAL1-like1 (AT1G26355.1 SP1L1)	Unknown	Unknown	339–360	351
	MDP0000322233	methionine sulfoxide reductase B5 (AT4G04830.1, ATMSRB5, MSRB5)	oxidation-reduction process	GO:0055114	128–149	140
	MDP0000380269	SPIRAL1-like1 (AT1G26355.1 SP1L1)	Unknown	Unknown	276–297	288
	MDP0000899071	(AT2G07820.1)	Unknown	Unknown	83–103	94
408a	MDP0000285733	DegP protease 9 (AT5G40200.1, DegP9)	proteolysis	GO:0006508	425–446	437
482a-3p	MDP0000134621	AAA-ATPase 1 (AT5G40010.1, AATP1)	ATP binding	GO:0005524	675–696	687
535a	MDP0000148556	receptor-like protein kinase 2 (RPK2, TOAD2, AT3G02130.1)	protein binding	GO:0005515	456–476	467

(*continued on next page*)

Table 1 (*continued*)

known miRNAs	Targets					
	Gene ID	Description	GO annotation	GO ID	Alignment Range	Cleavage Site
7125	MDP0000273257	zinc transporter 1 precursor (AT3G12750.1 ZIP1)	transmembrane transport	GO:0055085	133–153	144
828a/b	MDP0000124555	myb domain protein 66 (ATMYB66, MYB66, WER, WER1, AT5G14750.1)	DNA binding	GO:0003677	367–388	379
	MDP0000226215MDP0000253904MDP0000261265	myb domain protein 5 (ATMYB5, MYB5, AT3G13540.1)	DNA binding	GO:0003677	325–346	337
	MDP0000264051	myb domain protein 82 (AtMYB82, MYB82, AT5G52600.1)	DNA binding	GO:0003677	340–361	352
	MDP0000931057	high response to osmotic stress 10 (HOS10, MYB8, AT1G35515.1)	DNA binding	GO:0003677	367–388	379
	MDP0000578193	myb domain protein 66 (ATMYB66, MYB66, WER, WER1, AT5G14750.1)	DNA binding	GO:0003677	310–331	322
858	MDP0000031172MDP0000157940	myb domain protein 4 (ATMYB4, MYB4, AT4G38620.1)	DNA binding	GO:0003677	289–309	300
	MDP0000140609MDP0000887107	myb domain protein 12 (ATMYB12, MYB12, PFG1, AT2G47460.1)	DNA binding	GO:0003677	289–309	300
	MDP0000184538	myb domain protein 3 (ATMYB3, MYB3, AT1G22640.1)	DNA binding	GO:0003677	298–318	309
	MDP0000210851	myb domain protein 7 (ATMYB7, ATY49, MYB7, AT2G16720.1)	DNA binding	GO:0003677	289–309	300
	MDP0000318013	Duplicated homeodomain-like superfamily protein (ATMYB123, ATTT2, MYB123, TT2, AT5G35550.1)	DNA binding	GO:0003677	232–252	243
	MDP0000437717	Duplicated homeodomain-like superfamily protein (ATMYB123, ATTT2, MYB123, TT2, AT5G35550.1)	DNA binding	GO:0003677	292–312	303

Table 2
Detected targets of possible novel miRNAs and their reads counts in each stage of 'M9-T337' apple rootstock AR formation.

novel miRNAs	Mature sequence	Targets	Description	Reads counts		
		Gene ID		S0	S1	S2
chr1_1751510	AAUGACGGAUAGACGCCAAGGCGG	MDP0000879787	cytochrome P450, family 82, subfamily C, polypeptide 4 (AT4G31940.1, CYP82C4)	22	16	2
chr12_537666	ACAGGCGGGGGAUCAAAUAUGAAU	MDP0000742986	Protein kinase superfamily protein (AT1G54610.1)	57	0	0
chr15_1258354 chr2_1985756	UUGGACUGAAGGGAGCUCCC	MDP0000237553, MDP0000287069, MDP0000763497, MDP0000920127, MDP0000927314	TEOSINTE BRANCHED 1, cycloidea and PCF transcription factor 2 (AT4G18390.1, TCP2)	2106	1519	409
		MDP0000328318, MDP0000442611	TCP family transcription factor 4 (AT3G15030.1, MEE35, TCP4)			
chr3_2294129	UAACCGUCGUAAUGUCCCCCC	MDP0000180684	cytochrome P450, family 94, subfamily B, polypeptide 3 (AT3G48520.1, CYP94B3)	87	45	39
		MDP0000228366, MDP0000453190	cytochrome P450, family 94, subfamily B, polypeptide 1 (AT5G63450.1, CYP94B1)			
chr1_1772328	UGUGUUCUCAGGUCGCCCUUG	MDP0000130157, MDP0000259570	BR-signaling kinase 2 (AT5G46570.1, BSK2)	5810	2825	571
chr5_2661918		MDP0000243217, MDP0000380269	SPIRAL1-like1 (AT1G26355.1, SP1L1)			
		MDP0000290585	Integrase-type DNA-binding superfamily protein (AT2G40340.1, AtERF48, DREB2C)			
		MDP0000530255	Ctr copper transporter family (AT2G26975.1, COPT6)			
		MDP0000580010	indole-3-acetic acid inducible 9 (AT5G65670.1, IAA9)			
chr9_3280442	AUGACAGAAGAUAGAGAGUAC	MDP0000119458, MDP0000193702	Squamosa promoter-binding protein-like (SBP domain) transcription factor family protein (AT1G69170.1)	141	80	32
		MDP0000170630	Squamosa promoter-binding protein-like (SBP domain) transcription factor family protein (AT5G50670.1)			
		MDP0000249364	acyl-CoA synthetase 5 (AT1G62940.1, ACOS5)			
chr11_325587	AGCGCCUAGCGUCUUUUAGAACCU	MDP0000136236	Hyaluronan/mRNA binding family (AT4G17520.1)	27	27	13
chr11_393429	AAUUGUGUGGUUGAGAUUGUGUGG	MDP0000186276	Pentatricopeptide repeat (PPR) superfamily protein (AT5G11310.1)	10	21	10
chr13_684076	AAGAGUGUGUGAAGCUUUUGAGAA	MDP0000119262	GDSL-like Lipase/Acylhydrolase superfamily protein (AT3G26430.1)	74	161	64
chr13_741720, chr5_2611393	AUUCUAACUUUGGCAUCGGAGGUU	MDP0000218759	Unknown	12	17	6
chr17_1591707	GGAUGAACGGAUGAUGAACGAUGG	MDP0000256619, MDP0000722046, MDP0000884993	ADP glucose pyrophosphorylase 1 (AT5G48300.1, ADG1, APS1)	4	17	10
chr2_2025005	AGGAGAGACUUAGGGUUUGUGAGG	MDP0000301951	Ribosomal protein L22p/L17e family protein (AT1G27400.1)	16	26	12
chr2_2049428, chr6_2675036, chr5_2491757, chr10_189613	AUUGGCUUCUGAUGUCGACACGUG	MDP0000175052	DCD (Development and Cell Death) domain protein (AT5G42050.1)	143	242	82
chr5_2527345	UAGAUGAGUUUGAAUUUCGAGAUU	MDP0000892408	tetratricopeptide repeat (TPR)-containing protein (AT1G02910.1, LPA1)	15	28	10
chr6_2685738, chr14_1025887, chr13_674464	UGGCGGCGAUGCUCUCUAAUGAAG	MDP0000129520	phytochrome kinase substrate 1 (AT2G02950.1, PKS1)	65	65	42
chr8_3135214	AUUGGCUUCUGAUGUUGACACGUG	MDP0000265706	DHHC-type zinc finger family protein (AT1G69420.1)	126	188	85
chr8_3150848	AGAUGUGACAUCUUCUCUGGAAGU	MDP0000166111	Actin-like ATPase superfamily protein (AT1G13180.1, ARP3, ATARP3, DIS1)	24	23	6
chr9_3283476	GAACGGAUCUUCAAGGGCUUUUGG	MDP0000211491	Leucine-rich repeat protein kinase family protein (AT3G47570.1)	19	38	16

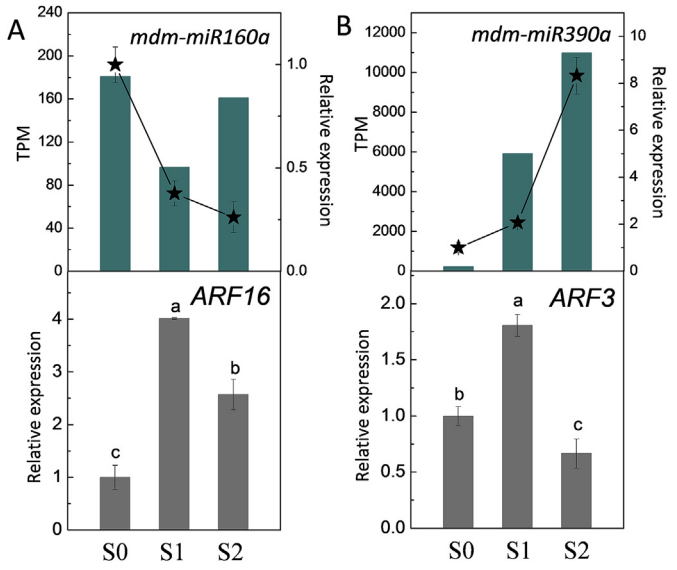

Fig. 5. Identification by qRT-PCR of differentially expressed miRNAs and their targets directly associated with auxin signal in AR formation. (A) Expression level of miR160a and its target genes. (B) Expression level of miR390a and its target genes. Blue bars refer to the TPM values of miRNA, the star-lines refer to the miRNA expression level identified by qRT-PCR, and the gray bars refer to targets expression levels identified by qRT-PCR. Bars show SD with three biological replicates. Values represent means ± SE (n = 3). The statistical analysis was performed by Duncan's multiple range test at level $p \leq 0.05$. (For interpretation of the references to color in this figure legend, the reader is referred to the Web version of this article.)

shown to regulate root stem cell niche maintenance and effect on root elongation (Zhao et al., 2014). Furthermore, sulfate is also associated with hormone metabolism, in brassicales plants, auxin-dependent regulation of root growth and branching involves the glucosinolate pathway, which is regulated by S depletion (Honsel et al., 2012). In the current study, *APS1* expression level has a similar expression pattern as IAA levels, indicating that miR395-*APS1* may be involved in sulfate-regulated AR formation. The results suggest that miR395 may took part in AR formation by targeting *APS1* to regulate S homeostasis, which was associated with auxin signaling. Therefore, nutrient homeostasis may be one of the induction factors of AR formation in apple rootstock.

In Arabidopsis, *pyr/pyl* mutant exhibited reduced sensitivity to ABA and reduced root hydrotropic response, and the expression of *PYL4* was demonstrated initiated a reprogramming of cellular metabolism (Antoni et al., 2013). A member of the miR398 family, miR398b, was identified in the degradome library that targets *PYL4* (*PCAR10*) (Table 1), which encodes proteins that function as ABA sensors and mediate ABA-dependent regulation of protein phosphate 2Cs (Pizzio et al., 2013). The expression patterns of miR398a and miR398b, however, are opposite of each other. Therefore, the results suggest that the miR398 family (miR398a and miR398b) may balance stress and regulate AR formation.

The degradome sequencing conducted in the present study revealed that the post-transcriptional regulated target of miR408a was *DegP9*. *Degp9* can mediate the degradation of *ARR4* and regulate the cross-talk between CTK and light-signaling pathways (Chi et al., 2016). Furthermore, type-A ARRs alter the pattern of cell division and differentiation in the stem cell niche of the root apical meristem by altering *PIN* levels, which intersects with cytokinin and auxin regulatory pathways (Zhang et al., 2011). These reports and the results obtained in the present study also infer that miR408 plays an important role in AR formation.

4.4. MiRNAs and their targets that are associated with cell fate determination, proliferation, and enlargement are involved in regulating AR formation

Five major differentially expressed miRNAs, miR171, miR156, miR166, miR319 and miR396, which are associated with cellular events such as cell fate determination, proliferation and enlargement, were identified within the degradome library. MiR171 is a relatively conserved miRNA present within different plant species that has been associated with root organ development. For example, miR171 up-regulated and enriched in *Solanum tuberosum* roots responding to drought (Hwang et al., 2011). *GRAS* TFs (*DELLA, HAM, SCR*, and others) are involved in regulating root growth, as well as the mediation of cell fate (Helariutta et al., 2000). In addition, miR171c regulated shoot apical meristem (SAM) development by *HAM* with *WOX4* in a *WUS-CLV* feedback loop (Fan et al., 2015). In the current study, *HAM3* (also named *LOM3, SCL6-IV,* and as a member of the GRAS protein family) was determined to be specifically targeted by miR171 (Table 1). Overall, the data suggest that miR171/*HAM* may interact with *WOX* to participate in cell fate determination during AR formation in apple rootstock.

In *Malus xiaojinensis,* auxin-induced AR formation relies on a relatively high expression of miR156 (Xu et al., 2017). However, miR156 expression in *Eucalyptus grandis* does not regulate AR induction (Levy et al., 2014). Therefore, miR156 regulated root development may be species specific. Alternatively, miR156 may be necessary but not a determining factor for AR induction in woody plants. In the present study, the target genes of miR166 have been verified to encode class III homeodomain zipper (*HD-ZIP*) TFs (including *PHB* and *REV*), which were also identified in the degradome library (Table 1). In Arabidopsis, *PHB* contributes to root vascular patterning and the differentiation of xylem cell types by directly binding to promoters of *MP/ARF5* and *IAA20* (Muller et al., 2016). *PHB* directly activates *IPT7* (CTK biosynthesis gene), and then CTK feeds back to repress *PHB* and microRNA, thus balancing the ratio of cell division with differentiation during root development (Dello Ioio et al., 2012). Collectively, all of the evidences and results also strongly suggest that miR166/*HD-ZIP* plays a crucial role in vascular reconstitution during AR formation.

The data obtained from the degradome library in the present study indicates that the targets of miR319 are genes encoding *TCP*, specifically *TCP2* and *TCP4*. *TCP* affects the morphogenesis of lateral organs, JA biosynthesis, and cell proliferation (Zhao et al., 2015). MiR396 regulates cell proliferation in meristems in Arabidopsis and roots of *Medicago truncatula* by targeting the growth-regulatory factors, *GRF1, GRF2,* and *GRF5* (Bazin et al., 2013). It has been demonstrated that miR396a regulates both the conversion of stem cells and root growth in the elongation zone of Arabidopsis roots instead of the meristem (Bao et al., 2014), suggest that miR396/GRF plays vital roles in both cell proliferation and enlargement. In addition, miR319/*TCP* also had different regulatory mechanisms in tomato roots vs. leaves (Ori et al., 2007). Thus, it appears that the regulatory networks of miR319/*TCPs* interacting with miR396/GRFs have species and organ specificity. Overall, miR319a and miR396 established a complex and diverse regulatory network for fine-tune cell proliferation of AR formation in apple rootstock (Fig. 9). However, additional in-depth research is warranted and necessary to completely elucidate the specific mechanisms regulating this response.

4.5. Differential expression of genes mediates AR formation

In the current study, auxin-related, cytokinin-related, stress signal response-related, cell cycle-related, and root development-related genes were identified within the sequencing database. The types of genes indicate that AR formation involves multiple biological pathways. In order to confirm the reliability of the sequencing results, some representative genes related with AR formation were examined by RT-

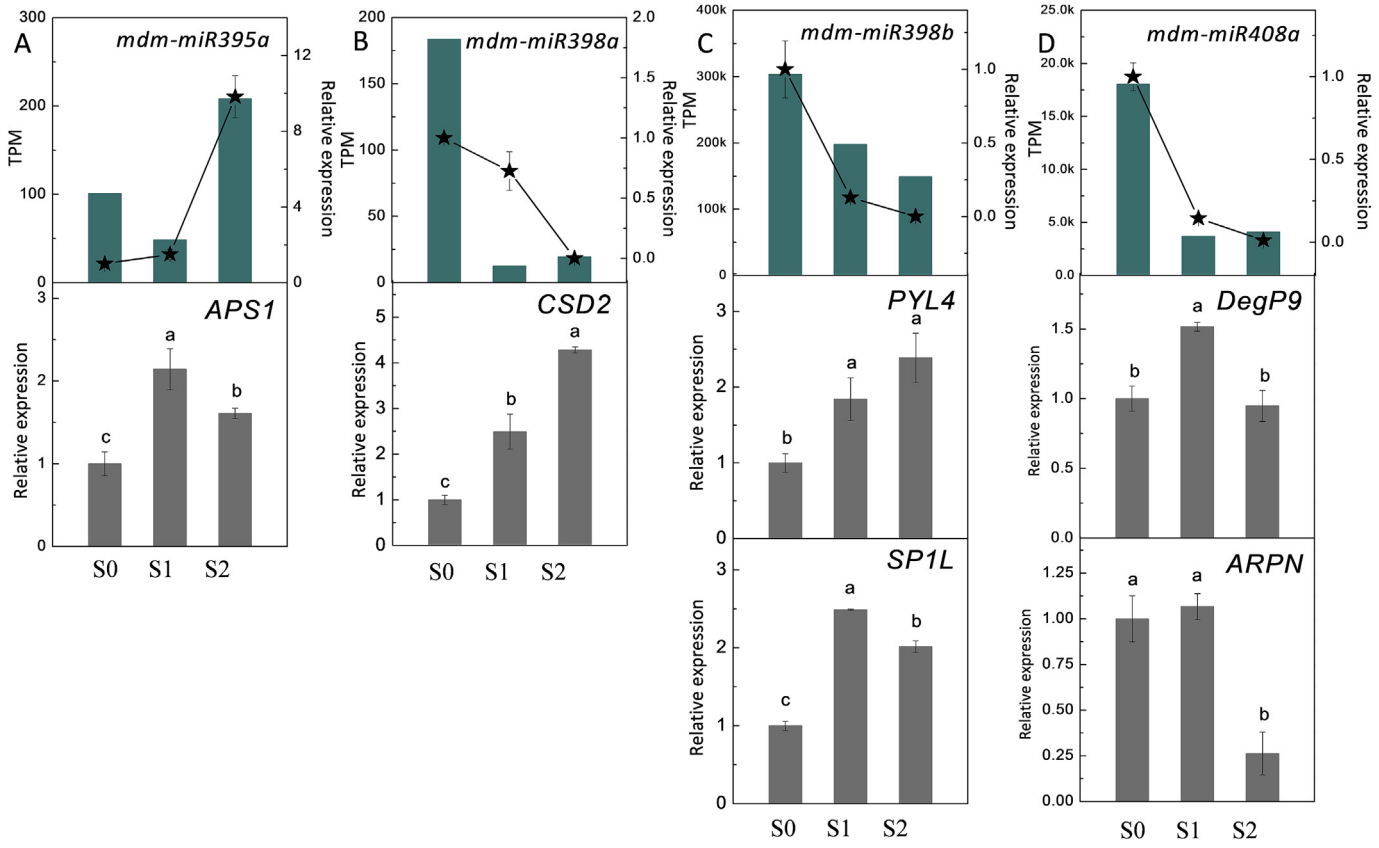

Fig. 6. Identification by qRT-PCR of differentially expressed miRNAs and their targets associated with stress response and signal transduction in AR formation. (A) Expression level of miR395a and its target genes. (B) Expression level of miR398a and its target genes. (C) Expression level of miR398b and its target genes. (D) Expression level of miR408a and its target genes. Blue bars refer to the TPM values of miRNA, the star-lines refer to the miRNA expression level identified by qRT-PCR, and the gray bars refer to targets expression levels identified by qRT-PCR. Bars show SD with three biological replicates. Values represent means ± SE (n = 3). The statistical analysis was performed by Duncan's multiple range test at level $p \leq 0.05$. (For interpretation of the references to color in this figure legend, the reader is referred to the Web version of this article.)

qPCR.

Root development is a dynamic process which requires the integration of plant hormones, transcriptional regulators, and small RNAs (Meng et al., 2010). For example, miR160 acts as a key controller of root cap cell formation through repression of the *AUXIN RESPONSE FACTOR (ARF)* genes, *ARF10* and *ARF16*, and also targets *ARF17* to regulate adventitious root initiation (Gutierrez et al., 2009). The transcription factors *SHR* (SHORT ROOT) and *SCR* (SCARECROW) have been identified as determining root cell fate (Carlsbecker et al., 2010). In the current study, Results of RT-qPCR analyses determined that the expression level of genes and miRNAs were induced during AR formation. In addition, hormone levels also changed over the course of AR formation. These data suggest that the aforementioned genes and miRNAs may interact with hormones to regulate AR induction, elongation, and development.

5. Conclusion

Base on the high-throughput sequencing and the degradome library, iconic miRNAs that are known to be auxin-related, stress response-related, and cell fate-related were identified within the database generated in present study. The range of differentially expressed miRNAs, and the range of target genes that are regulated by the miRNAs, clearly indicated that AR development in apple rootstocks is a complex biological process. We have used the collective data on AR development to construct a model of the interacting response mechanisms regulating AR formation in 'M9-T337' apple rootstocks (Fig. 9). Many auxin-, stress response-, and cell fate-related miRNAs and genes interact with hormones signaling to ultimately control AR formation (Fig. 9). Our study provides an overview of the transcriptomic changes that occur during AR formation in 'M9-T337' apple rootstocks. It will be a foundation for the further exploration of candidate miRNAs and genes, along with their associated pathways, that regulate AR formation. However, owing to technical limitations, post-transcriptional or (post)-translational evidence for AR formation still needs further analysis and experimentally demonstrated.

List of abbreviations

AUX:auxin; CTK: cytokinin; IAA: Indole-3-acetic acid; ZR: zeatin riboside; GA: gibberellin; BR: brassinolide; JA: jasmonic acid; ABA: abscisic acid; AR: adventitious root.

Author contributions

DZ, LX, CZ and KL designed and interpreted of all experiments. KL, DZ, ZL, LX and LB participated in the experimental design and data analysis. KL, ZL, LX, YW and JM performed the hormone and measurements. KL, DZ, ZL, LX, JM, YM and YW performed material sampling and the laboratory data measurements. KL, DZ, ZL and XL participated in the preparation of the manuscript. All authors have read and approved the manuscript.

Conflicts of interest

The authors declare that they have no competing interests.

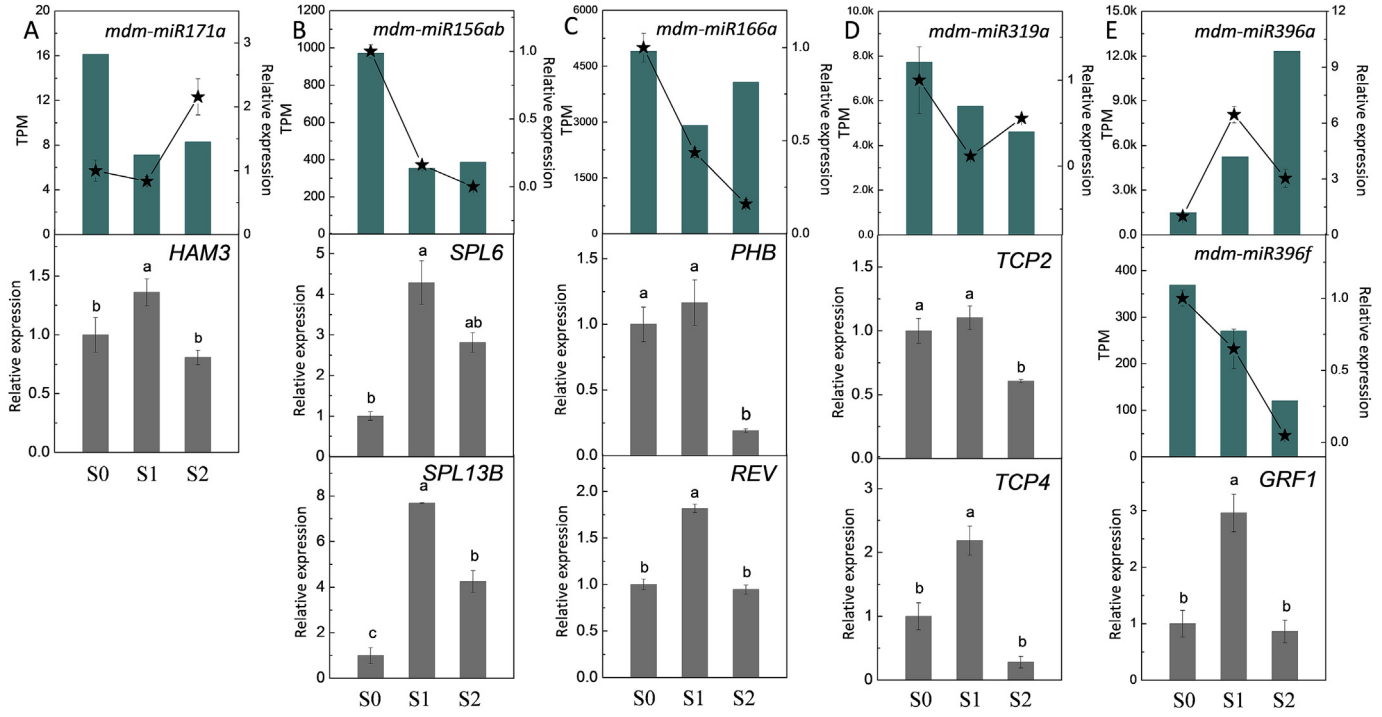

Fig. 7. Identification by qRT-PCR of differentially expressed miRNAs and their targets associated with cell fate transformation, proliferation and enlargement in AR formation. (A) Expression level of miR171a and its target genes. (B) Expression level of miR156ab and its target genes. (C) Expression level of miR166a and its target genes. (D) Expression level of miR319a and its target genes. (E) Expression level of miR396a and miR396f and their target gene. Blue bars refer to the TPM values of miRNA, the star-lines refer to the miRNA expression level identified by qRT-PCR, and the gray bars refer to targets expression levels identified by qRT-PCR. Bars show SD with three biological replicates. Values represent means ± SE (n = 3). The statistical analysis was performed by Duncan's multiple range test at level $p \leq 0.05$. (For interpretation of the references to color in this figure legend, the reader is referred to the Web version of this article.)

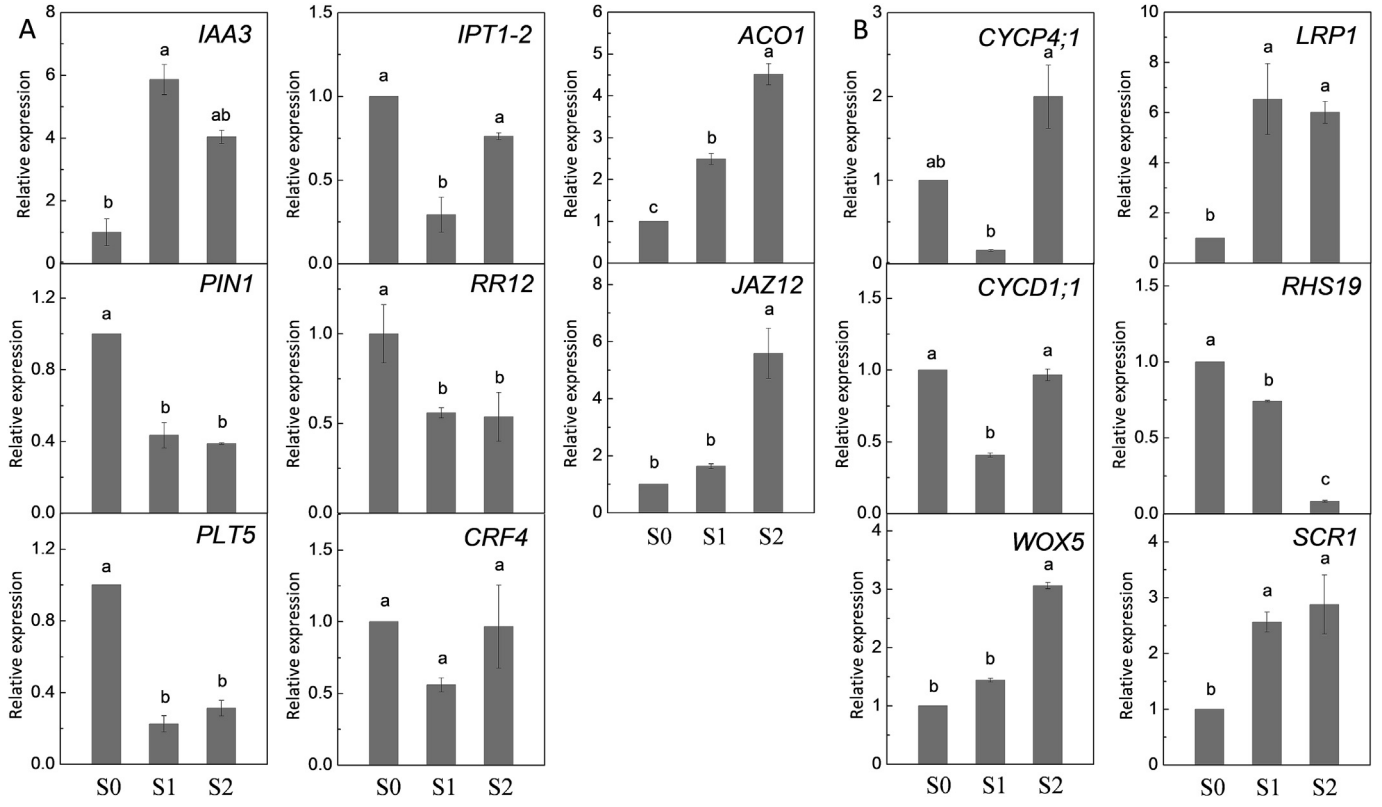

Fig. 8. Identification by qRT-PCR of downstream key genes associated with related pathways in AR formation. (A) Expression level of genes related with phytohormone pathways. (B) Expression level of genes related with cellular events. Bars show SD with three biological replicates. Values represent means ± SE (n = 3). The statistical analysis was performed by Duncan's multiple range test at level $p \leq 0.05$.

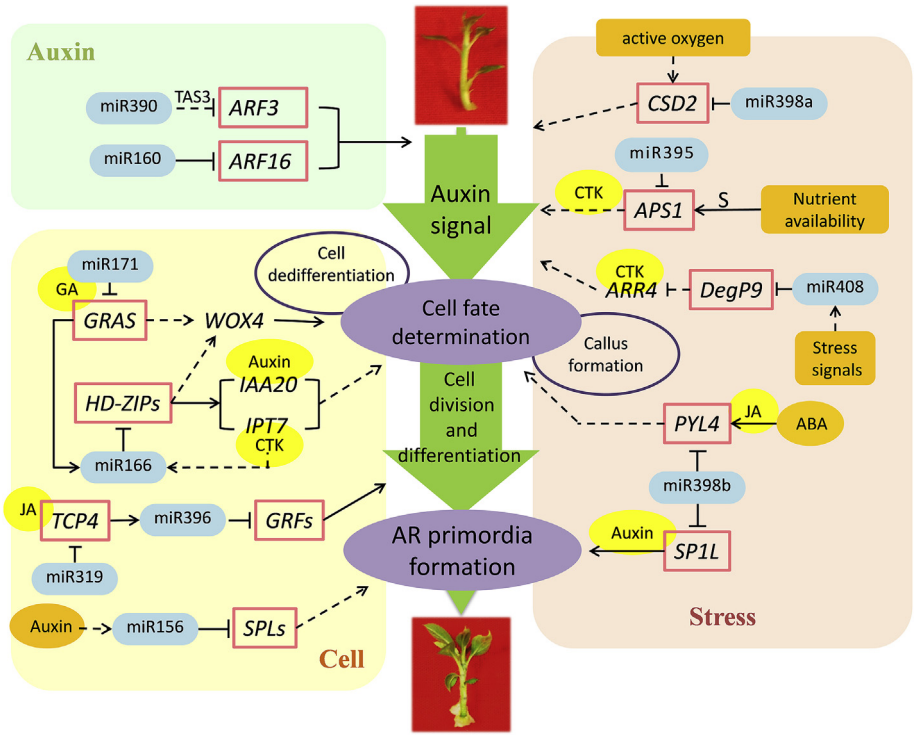

Fig. 9. Hypothetical model of miRNAs regulating AR formation through the pathways of auxin, stress and cellular events in stem cuttings of 'M9-T337' apple rootstock.

Acknowledgments

This work was financially funded by Shaanxi province key research and development program (2017NY0055), Yangling Demonstration Zone Science and Technology Plan Project (2018NY-08), the China Apple Research System (CARS-27), Tang Scholar by Cyrus Tang Foundation and Northwest A&F University, Yangling Subsidiary Center Project of the National Apple Improvement Center.

Appendix A. Supplementary data

Supplementary data to this article can be found online at https://doi.org/10.1016/j.plaphy.2019.03.006.

References

Addoquaye, C., Miller, W., Axtell, M., 2009. CleaveLand: a pipeline for using degradome data to find cleaved small RNA targets. Bioinformatics 25 (1), 130–131.

Antoni, R., Gonzalez-Guzman, M., Rodriguez, L., Peirats-Llobet, M., Pizzio, G.A., Fernandez, M.A., et al., 2013. PYRABACTIN RESISTANCE1-LIKE8 plays an important role for the regulation of abscisic acid signaling in root. Plant Physiol. 161 (2), 931–941.

Bao, M.L., Bian, H.W., Zha, Y.L., Li, F.Y., Sun, Y.Z., Bai, B., et al., 2014. miR396a-Mediated basic helix-loop-helix transcription factor bHLH74 repression acts as a regulator for root growth in Arabidopsis seedlings. Plant Cell Physiol. 55 (7), 1343–1353.

Bazin, J., Khan, G.A., Combier, J.P., Bustos-Sanmamed, P., Debernardi, J.M., Rodriguez, R., et al., 2013. miR396 affects mycorrhization and root meristem activity in the legume Medicago truncatula. Plant J. 74 (6), 920–934.

Carlsbecker, A., Lee, J.Y., Roberts, C.J., Dettmer, J., Lehesranta, S., Zhou, J., et al., 2010. Cell signalling by microRNA165/6 directs gene dose-dependent root cell fate. Nature 465 (7296), 316–321.

Chen, Z.H., Bao, M.L., Sun, Y.Z., Yang, Y.J., Xu, X.H., Wang, J.H., et al., 2011. Regulation of auxin response by miR393-targeted transport inhibitor response protein 1 is involved in normal development in Arabidopsis. Plant Mol. Biol. 77 (6), 619.

Chi, W., Li, J., He, B.Y., Chai, X., Xu, X.M., Sun, X.W., et al., 2016. DEG9, a serine protease, modulates cytokinin and light signaling by regulating the level of arabidopsis response regulator 4. Proc. Natl. Acad. Sci. U. S. A 113 (25), E3568–E3576.

Da Costa, C.T., Gaeta, M.L., Ernesto, D.A.M.J., et al., 2018. Comparative adventitious root development in pre-etiolated and flooded, Arabidopsis, hypocotyls exposed to different auxins. Plant Physiol. Biochem. 127, 161–168.

Dello Ioio, R., Galinha, C., Fletcher, A.G., Grigg, S.P., Molnar, A., Willemsen, V., et al., 2012. A PHABULOSA/cytokinin feedback loop controls root growth in Arabidopsis. Curr. Biol. 22 (18), 1699–1704.

Fan, S., Zhang, D., Lei, C., Chen, H.F., Xing, L.B., Ma, J.J., Zhao, C.P., Han, M.Y., 2016. Proteome analyses using itraq labeling reveals critical mechanisms in alternate bearing malus prunifolia. J. Proteome Res. 15, 3602–3616.

Fan, T., Li, X.M., Yang, W., Xia, K.F., Jie, O.Y., Zhang, M.Y., 2015. Rice osa-miR171c mediates phase change from vegetative to reproductive development and shoot apical meristem maintenance by repressing four OsHAM transcription factors. PLoS One 10 (5).

Feng, S.J., Xu, Y.M., Guo, C.K., Zheng, J.R., Zhou, B.Y., Zhang, Y.T., et al., 2016. Modulation of miR156 to identify traits associated with vegetative phase change in tobacco (Nicotiana tabacum). J. Exp. Bot. 67 (5), 1493–1504.

Fridovich, I., 1995. Superoxide radical and superoxide dismutases. Annu. Rev. Biochem. 64, 97–112.

Friedlander, M.R., Mackowiak, S.D., Li, N., Chen, W., Rajewsky, N., 2012. miRDeep2 accurately identifies known and hundreds of novel microRNA genes in seven animal clades. Nucleic Acids Res. 40 (1), 37–52.

Gutierrez, L., Bussell, J.D., Pacurar, D.I., Schwambach, J., Pacurar, M., Bellini, C., 2009. Phenotypic plasticity of adventitious rooting in Arabidopsis is controlled by complex regulation of AUXIN RESPONSE FACTOR transcripts and MicroRNA abundance. Plant Cell 21 (10), 3119–3132.

Helariutta, Y., Fukaki, H., Wysocka-Diller, J., Nakajima, K., Jung, J., Sena, G., et al., 2000. The SHORT-ROOT gene controls radial patterning of the Arabidopsis root through radial signaling. Cell 101 (5), 555–567.

Honsel, A., Kojima, M., Haas, R., Frank, W., Sakakibara, H., Herschbach, C., et al., 2012. Sulphur limitation and early sulphur deficiency responses in poplar: significance of gene expression, metabolites, and plant hormones. J. Exp. Bot. 63 (5), 1873–1893.

Hwang, E.W., Shin, S.J., Yu, B.K., Byun, M.O., Kwon, H.B., 2011. miR171 family members are involved in drought response in Solanum tuberosum. J. Plant Biol. 54 (1), 43–48.

Levy, A., Szwerdszarf, D., Abu-Abied, M., Mordehaev, I., Yaniv, Y., Riov, J., et al., 2014. Profiling microRNAs in Eucalyptus grandis reveals no mutual relationship between alterations in miR156 and miR172 expression and adventitious root induction during development. BMC Genomics 15, 524.

Liang, G., Yang, F.X., Yu, D.Q., 2010. MicroRNA395 mediates regulation of sulfate accumulation and allocation in Arabidopsis thaliana. Plant J. 62 (6), 1046–1057.

Liu, Z.H., Li, J., Wang, L., Li, Q., Lu, Q., Yu, Y.C., et al., 2016. Repression of callus initiation by the miRNA-directed interaction of auxin-cytokinin in Arabidopsis thaliana. Plant J. 87 (4), 391–402.

Livak, K.J., Schmittgen, T.D., 2001. Analysis of relative gene expression data using real-time quantitative PCR and the 2(T)(-Delta Delta C) method. Methods 25 (4), 402–408.

Marin, E., Jouannet, V., Herz, A., Lokerse, A.S., Weijers, D., Vaucheret, H., et al., 2010. miR390, Arabidopsis TAS3 tasiRNAs, and their AUXIN RESPONSE FACTOR targets define an autoregulatory network quantitatively regulating lateral root growth. Plant Cell 22 (4), 1104.

Meng, Y.J., Ma, X.X., Chen, D.J., Wu, P., Chen, M., 2010. MicroRNA-mediated signaling involved in plant root development. Biochem. Biophys. Res. Commun. 393 (3), 345–349.
Muller, C.J., Valdes, A.E., Wang, G.D., Ramachandran, P., Beste, L., Uddenberg, D., et al., 2016. PHABULOSA mediates an auxin signaling loop to regulate vascular patterning in Arabidopsis. Plant Physiol. 170 (2), 956–970.
Negishi, N., Nakahama, K., Urata, N., Kojima, M., Sakakibara, H., Kawaoka, A., 2014. Hormone level analysis on adventitious root formation in Eucalyptus globulus. N. For. 45 (4), 577–587.
Ori, N., Cohen, A.R., Etzioni, A., Brand, A., Yanai, O., Shleizer, S., et al., 2007. Regulation of LANCEOLATE by miR319 is required for compound-leaf development in tomato. Nat. Genet. 39 (6), 787–791.
Pizzio, G.A., Rodriguez, L., Antoni, R., Gonzalez-Guzman, M., Yunta, C., Merilo, E., et al., 2013. The PYL4 A194T mutant uncovers a key role of PYR1-LIKE4/PROTEIN PHOSPHATASE 2CA interaction for abscisic acid signaling and plant drought resistance. Plant Physiol. 163 (1), 441–455.
Rani, D.B., Taketa, S.M., 2005. Cytokinin inhibits lateral root initiation but stimulates lateral root elongation in rice (Oryza sativa). J. Plant Physiol. 162 (5), 507.
Steffens, B., Rasmussen, A., 2016. The physiology of adventitious roots. Plant Physiol. 170 (2), 603–617.
Sukumar, P., Maloney, G.S., Muday, G.K., 2013. Localized induction of the ATP-binding cassette B19 auxin transporter enhances adventitious root formation in Arabidopsis. Plant Physiol. 162 (3), 1392.
Wang, J.W., Wang, L.J., Mao, Y.B., Cai, W.J., Xue, H.W., Chen, X.Y., 2005. Control of root cap formation by MicroRNA-targeted auxin response factors in Arabidopsis. Plant Cell 17 (8), 2204–2216.
Xing, L., Zhang, D., Li, Y., Zhao, C., Zhang, S., Shen, Y., et al., 2014. Genome-wide identification of vegetative phase transition-associated microRNAs and target predictions using degradome sequencing in Malus hupehensis. BMC Genomics 15 (1), 1125.
Xu, X.Z., Li, X., Hu, X.W., Wu, T., Wang, Y., Xu, X.F., et al., 2017. High miR156 expression is required for auxin-induced adventitious root formation via MxSPL26 independent of PINs and ARFs in malus xiaojinensis. Front. Plant Sci. 8.
Yan, R., Qing, X., Liwei, W., et al., 2018. Involvement of metabolic, physiological and hormonal responses in the graft-compatible process of cucumber/pumpkin combinations was revealed through the integrative analysis of mRNA and miRNA expression. Plant Physiol. Biochem. 129, 368–380.
Zhang, W.J., To, J.P.C., Cheng, C.Y., Schaller, G.E., Kieber, J.J., 2011. Type-A response regulators are required for proper root apical meristem function through post-transcriptional regulation of PIN auxin efflux carriers. Plant J. 68 (1), 1–10.
Zhao, Q., Wu, Y., Gao, L., Ma, J., Li, C.Y., Xiang, C.B., 2014. Sulfur nutrient availability regulates root elongation by affecting root indole-3-acetic acid levels and the stem cell niche. J. Integr. Plant Biol. 56 (12), 1151–1163.
Zhao, W.C., Li, Z.L., Fan, J.W., Hu, C.L., Yang, R., Qi, X., et al., 2015. Identification of jasmonic acid-associated microRNAs and characterization of the regulatory roles of the miR319/TCP4 module under root-knot nematode stress in tomato. J. Exp. Bot. 66 (15), 4653–4667.
Zhou, L., Hou, H., Yang, T., et al., 2018. Exogenous hydrogen peroxide inhibits primary root gravitropism by regulating auxin distribution during Arabidopsis seed germination. Plant Physiol. Biochem. 128, 126–133.
Zuo, X., Zhang, D., Wang, S., et al., 2018. Expression of genes in the potential regulatory pathways controlling alternate bearing in 'Fuji' (Malus domestica Borkh.) apple trees during flower induction. Plant Physiology and Biochemistry. 2018 132, 579–589.